Implementation of a Spacer Grid Rod Thermal Hydraulic Reconstruction (ROTHCON) Capability into the Thermal Hydraulic Subchannel Code CTF

Robert K. Salko,[*,a] William D. Pointer,[a] Marc-Oliver Delchini,[a] William L. Gurecky,[b] Kevin T. Clarno,

[a]*Oak Ridge National Laboratory*
1 Bethel Valley Road
Oak Ridge, TN 37830

[b]*University of Texas at Austin*
Pickle Research Campus, R-9000
Austin, Texas 78712

[c]*University of Michigan*
1906 Cooley Bldg.
2355 Bonisteel Blvd.
Ann Arbor, MI 48109-2104

[*]Email: salkork@ornl.gov

Number of pages: 23
Number of tables: 1
Number of figures: 11

Abstract

The Consortium for Advanced Simulation of Light Water Reactors (CASL) is developing a core simulator capability known as the Virtual Environment for Reactor Applications (VERA) to address nuclear industry challenge problems such as crud-induced power shift (CIPS). CTF is the thermal-hydraulics subchannel code that provides thermal feedback in the coupled neutronics, thermal-hydraulics, crud-chemistry simulation that VERA performs. It has been discovered that the coarse meshing approach used by CTF (in which fuel rods are discretized into four azimuthal segments) can be a source of error in predicting crud growth and boron distribution in VERA CIPS calculations. Spacer grid effects lead to complex rod-to-fluid heat transfer behavior that, when not resolved, can lead to error in the prediction of crud growth and boron deposition. A higher-fidelity computational fluid dynamics approach can be used instead of CTF, but this leads to excessive simulation times. This paper presents an approach for using high-fidelity CFD data to create shape functions that are used in CTF to reconstruct rod surface heat transfer behavior as a function of spacer grid geometry. The approach is demonstrated for a 5×5 rod bundle facility with five mixing vane grids under a range of operating conditions encountered in nominal pressurized water reactor conditions. It is demonstrated that the grid heat transfer maps are successful at introducing a higher fidelity heat transfer modeling capability into CTF.

Keywords — hi2lo, ROTHCON, CTF, CFD-informed, subchannel

I. INTRODUCTION

CTF [1] is a two-fluid, three-field subchannel thermal-hydraulics code which is a derivative of the legacy subchannel code COBRA-TF [2]. It is being jointly developed by Oak Ridge National Laboratory and North Carolina State University as part of the Consortium for Advanced Simulation of Light Water Reactors (CASL) program. CTF has been incorporated into the Virtual Environment for Reactor Applications (VERA), which is a high-fidelity multiphysics reactor core simulator capability developed by CASL. In VERA, CTF has been coupled to the neutronics code MPACT [3] and the crud chemistry code MAMBA [4]. VERA is being developed to model pressurized water reactor (PWR) and boiling water reactor (BWR) reactor depletions, departure from nucleate boiling (DNB), crud-induced power shift (CIPS), and reactivity insertion accident (RIA). This work focuses on implementing grid modeling improvements in CTF for improved modeling of the CIPS challenge problem.

Past studies [5, 6] have shown that the differences in mesh resolution between a subchannel approach and a computational fluid dynamics (CFD) approach can lead to discrepancies in the prediction of total deposition of crud and boron on fuel rod surfaces when performing coupled thermal-hydraulics and crud chemistry simulations. The discrepancies are primarily the result of boiling, which is the primary driver for crud deposition and a localized effect. The subchannel modeling approach traditionally uses the pins as the basis for the mesh cell boundaries, which leads to a rod discretization of four azimuthal sectors per rod. The CFD approach uses a much more highly resolved mesh, which leads to better resolution of physical phenomena. In addition to the better mesh resolution, the CFD code can model explicit spacer grid geometry and fluid turbulence behavior that will allow it to capture spacer grid dependent heat transfer effects.

For a simulation of nominal light water reactor (LWR) conditions, the surface of the rod experiences non-negligible gradients in local rod surface temperature around the azimuth of the rod at a given axial location. Even with properly calibrated closure models, a subchannel code will only be able to predict an average rod surface temperature at a given level, missing the peaks and valleys in the temperature profile. It may be that the average temperature is slightly below the saturation temperature, which leads to no boiling and prevents any crud from being grown.

This work described in this paper looks to develop an approach for using CFD simulation data to

This manuscript has been authored by UT-Battelle, LLC, under contract DE-AC05-00OR22725 with the US Department of Energy (DOE). The US government retains and the publisher, by accepting the article for publication, acknowledges that the US government retains a nonexclusive, paid-up, irrevocable, worldwide license to publish or reproduce the published form of this manuscript, or allow others to do so, for US government purposes. DOE will provide public access to these results of federally sponsored research in accordance with the DOE Public Access Plan (http://energy.gov/downloads/doe-public-access-plan).

capture rod bundle and spacer grid geometry effects on rod heat transfer effects. The approach will be outlined in Section II, a rod bundle model will be developed in Section III to demonstrate the approach, and results will be assessed in Section IV.

II. APPROACH

To address the issues identified in Section I, a process called ROTHCON, which stands for Rod thermal-hydraulic reconstruction, was developed and implemented into CTF. The goal of this process is to capture the shape of the high-fidelity thermal-hydraulics (T/H) solution predicted by the commercial CFD code STAR-CCM+ as a function of grid geometry. It is assumed that the shape function will be independent of operating conditions so that a model developed for a certain spacer grid type can be reused every time the impact of that spacer grid needs to be modeled.

This concept has been used in the past for capturing grid spacer heat transfer effects by developing reduced-order shape functions from experimental data in Yao-Hochreiter-Leech (YHL) [7]. Work was done by [8] to extend this concept by using CFD data in place of experimental data for developing the rod heat transfer shape function. Shape functions were developed for each CTF rod surface for a rod bundle subregion to demonstrate this approach.

The work described here further develops on this concept in several ways:

- Rather than develop shape functions for the specific CTF mesh, a map of high-resolution enhancement factors are generated from the CFD data and a method is implemented into CTF for mapping that data to a rod surface mesh that is independent of the original CTF rod surface mesh. This mesh may be much finer than the CTF mesh, which is important for resolving localized T/H behavior that is important in crud-induced localized corrosion (CILC) analysis.

- The effect of operating conditions and power distribution on the effectiveness of the approach is tested.

- The process for extracting CFD data and developing the enhancement maps is formalized so that it can be applied for full rod bundle geometry including multiple spacer grids.

The YHL model provides a multiplier on bare-bundle, single-phase heat transfer coefficient (HTC) as a function of general grid geometry (i.e., blockage ratio). While the model is a general purpose model and can provide average heat transfer enhancement predictions, it cannot be used to capture localized heat transfer effects, and predictions will have limited accuracy for specific grid designs.

The YHL approach could be improved by using data from the exact grid design to develop the shape function. Because experiments are expensive to run and offer a limited amount of data to calibrate the model, an alternative is to use a validated CFD code to generate the high-fidelity data. CFD can be used to generate a library of data for different spacer grid designs; then the user can point to this library from the subchannel model, tying grids in the subchannel code to grids in the library file.

Specifically, the approach is to generate an HTC multiplier map as defined in Equation 1.

$$M(z-z_g,\theta) = \frac{Nu(z-z_g)}{Nu_0} \tag{1}$$

Where Nu_0 is the Nusselt number for a bare region of the model with no grid heat transfer effects, and Nu is the Nusselt number for a region of the model with grid heat transfer effects. The equation specifies that the multiplier is a function of space—both downstream distance from the spacer grid ($z - z_g$), and at the azimuthal location on the rod's surface (θ).

The multiplier, M, will be developed from tabular data produced by the CFD code using Equation 2, where M is the HTC multiplier, q'_{CFD} is the local STAR-CCM+ heat flux, $T_{w,\text{CFD}}$ is the local STAR-CCM+ rod surface temperature, $T_{b,\text{CFD}}$ is the mass flow rate averaged fluid temperature adjacent to the rod's surface, and h_{bare} is the local HTC when no grids are present.

A STAR-CCM+ simulation was not run without grids to produce h_{bare}, so a workaround was to run CTF with no grid effects and use the CTF HTC ($h_{\text{bare, CTF}}$) to normalize the STAR-CCM+ results. As it has been shown previously [9], CTF and subchannel-averaged STAR-CCM+ bare-bundle HTC predictions for single-phase flow are very agreeable, so this is a valid work-around. Furthermore, the multiplier maps were generated using a uniform axial heat flux simulation in STAR-CCM+ so that the multiplier maps are not a function of heat flux shape. This same approach has been used as described in Salko [9] to reconstruct turbulent kinetic energy on the rod's surface, which is also a boundary condition to MAMBA.

$$M = \frac{q''_{\text{CFD}}/(T_{w,\text{CFD}} - T_{b,\text{CFD}})}{h_{\text{bare, CTF}}} \tag{2}$$

In addition to modifying CTF to read and use the CFD-predicted multipliers, a feature was also implemented to allow the user to refine the rod surface mesh that is used to couple CTF to MAMBA, as shown in Figure 1. In this figure, the bottom-most mesh is the CFD mesh, the top-most mesh is the traditional CTF mesh, and the middle mesh is the coupling mesh. The coupling between CTF and MAMBA

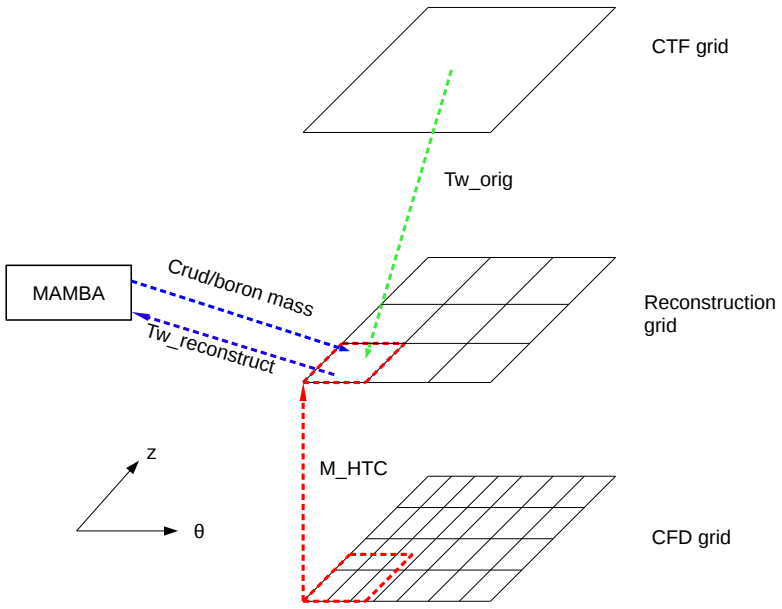

Fig. 1. Example of how a CFD multiplier map is remapped to the CTF reconstruction mesh and passed to MAMBA.

[4] is achieved by running CTF until a steady T/H solution is obtained. MAMBA is then run for a depletion timestep using that T/H solution as the boundary condition. The reconstruction approach was implemented by calculating a new rod surface temperature field on the coupling mesh using the bulk T/H solution from CTF and the multiplier map from CFD prior to calling MAMBA.

The heat transfer coefficient is calculated by CTF using a wall heat partitioning model that considers both single-phase convection and boiling heat transfer as separate effects. The CFD heat transfer multipliers are numerically integrated over the bounds of the coupling mesh cell and applied to the single-phase convection component of heat transfer only. An iterative solution is used to converge on the correct HTC/rod temperature pair for each node in the coupling mesh.

III. MODEL

A test geometry was needed to demonstrate the approach. The Westinghouse 5 $\times$ 5 rod bundle experiments were a series of electrically heated rod bundle experiments performed at the Columbia University Heat Transfer Research Facility in the 1980s. These tests served as the basis for the geometry because

TABLE I
Operating conditions used in this study.

Case	Outlet pressure (bar)	Inlet temperature (°C)	Mass flux ($kg\,m^{-1}\,s^{-2}$)	Heat rate ($kW\,m^{-1}$)
0	159.9	292.7	3684.0	18.26
1	159.9	310.8	3647.2	18.26
2	159.9	292.7	3131.5	18.26
3	159.9	292.7	4236.7	18.26
4	159.9	292.7	3684.0	18.26
5	159.9	292.7	3684.0	22.82

detailed computer-aided drafting (CAD) drawings were readily available for generating the STAR-CCM+ model. The 5×5 array included all rods of the same dimension. An example of the lateral geometry is shown in Figure 2(a). The radial power distribution in the facility was nonuniform in the radial direction, with 6 of the center 9 rods being at a slightly higher power than the rest of the rods. The axial power shape was uniform. Specific dimensions and pin power factors have been redacted from the figure due to the proprietary nature of the data.

The model consists of five mixing vane grids in the heated length of the model. Grid span lengths are consistent with lengths in actual PWR fuel assemblies, although the heated length is slightly shorter than that of a typical PWR. An example of the mixing vane grid is shown in Figure 2(b). Outlet temperature measurements and rod surface temperature measurements were made in this facility, along with pressure drop measurements. However, no comparison with experimental results is being made in this paper. Operating conditions were arbitrarily selected to represent nominal PWR operating conditions (Case 0), with perturbations on inlet flow, inlet temperature, power shape, and power level. Operating conditions used for this study are summarized in Table I. In addition to Case 5 having a higher power, it also uses a nonuniform power shape that was extracted from a section of a VERA (neutronics coupled to thermal hydraulics) simulation of a 4-Loop PWR. A bundle section with a very steep power gradient was selected to test the effects of nonuniform power on the feature. Case 5 also encounters a significant amount of subcooled boiling for PWR conditions. The baseline case, Case 0, was used to generate the grid heat transfer shape function, which was then used by CTF for predicting temperatures in the remaining cases. The perturbation studies were performed to assess the applicability of the shape function to cases with varied operating conditions.

The STAR-CCM+ and CTF models were set up according to the geometry specification. A trimmed mesh with one prismatic extrusion layer was set up in STAR-CCM+ from the available CAD file. Some

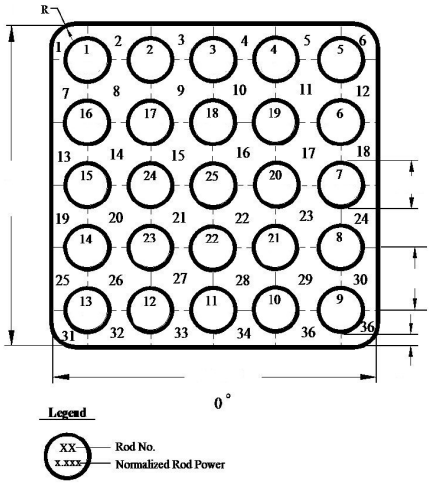

(a) Lateral geometry of the 5 × 5 rod bundle geometry used in Westinghouse tests.

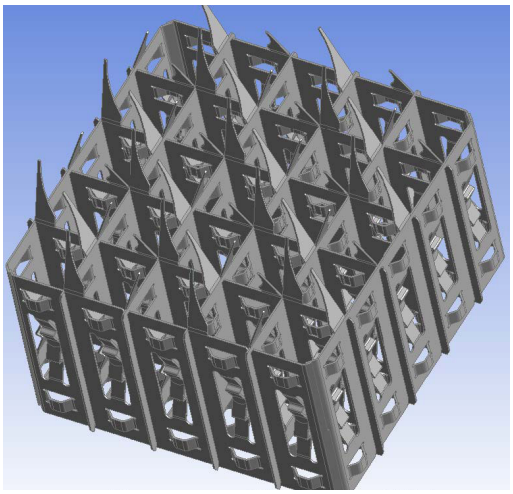

(b) CAD representation of the mixing vane grid used in the 5 × 5 tests.

Fig. 2. 5 × 5 facility geometry.

simplifications to the facility geometry were made: the regions where the springs and dimples contacted the rods were removed to relax meshing requirements. The total mesh cell count was roughly 19 million cells. The Eulerian-Eulerian dispersed phase model in STAR-CCM+ was used to allow for modeling boiling and two-phase flow in the CFD simulation. Considerably more details on how the STAR-CCM+ model was set up, including results of a grid convergence study for the geometry, can be found in a CASL milestone report on the model [10].

The CTF model was set up using the specification [11] for defining flow channel geometry, rod power distribution, and model boundary conditions. It is important that CTF be calibrated so that its baseline results are in good agreement with the STAR-CCM+ subchannel-averaged results. The heat transfer shape functions should not be offsetting errors in other subchannel closure models, so CTF was calibrated in three ways (1) by setting the fluid properties to match the values used in STAR-CCM+, (2) by back-calculating the form loss coefficients from STAR-CCM+ pressure drops, and (3) by calibrating the mixing coefficient to match the outlet temperature distribution of STAR-CCM+.

The grid form loss coefficients were calculated on a per-channel basis, and it was found that they varied less than 30 % from channel to channel. A comparison of the bundle-average pressure drop predicted by CTF and STAR-CCM+ is shown in Figure 3, which shows that agreement between the two codes is nearly perfect when compared to the calibrated grid form loss coefficients. Additional details pertaining to

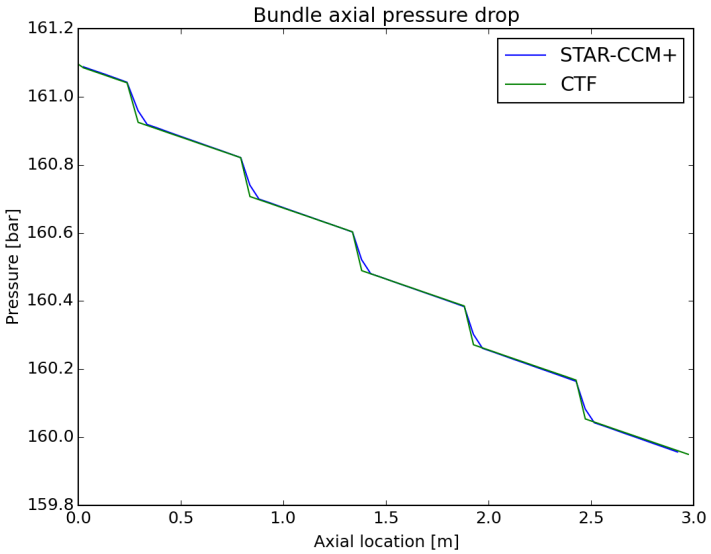

Fig. 3. Bundle average axial pressure distribution predicted by CTF and STAR-CCM+.

the form loss calibration can be found in [12].

CTF uses a simple turbulent diffusion model to approximate the effect of turbulence on the net mixing of mass, momentum, and energy from one channel to another. The model contains a tuning coefficient, β, known as the *mixing coefficient*. A nominal β value of 0.005 was used to generate base results. An in-depth study of calibrating the mixing coefficient using STAR-CCM+ results was documented by Gordon [13], which arrived at an optimal value of 0.037 for PWR rod-bundle conditions. Figure 4 shows the effect of calibrating the mixing coefficient on predicted subhcannel temperature distribution. CTF agrees more closely with STAR-CCM+ after the calibration.

IV. ASSESSMENT

IV.A. Coupling Mesh Refinement

A coupling mesh refinement study was performed to verify that the agreement between the supplied HTC multiplier map and the coupling mesh multiplier map continues to improve as the mesh is refined. The coupling mesh refinement is denoted as $n \times m$, where n is the number of divisions of a CTF rod sector into sub-sectors, and m is the number of divisions of a CTF rod level into sub-levels. A rod sector is defined as the azimuthal portion of the rod that connects to a single coolant subchannel, and a CTF rod level is defined as a level in the user-defined axial coolant mesh. CTF is run with coupling mesh refinement of 1×1 (no

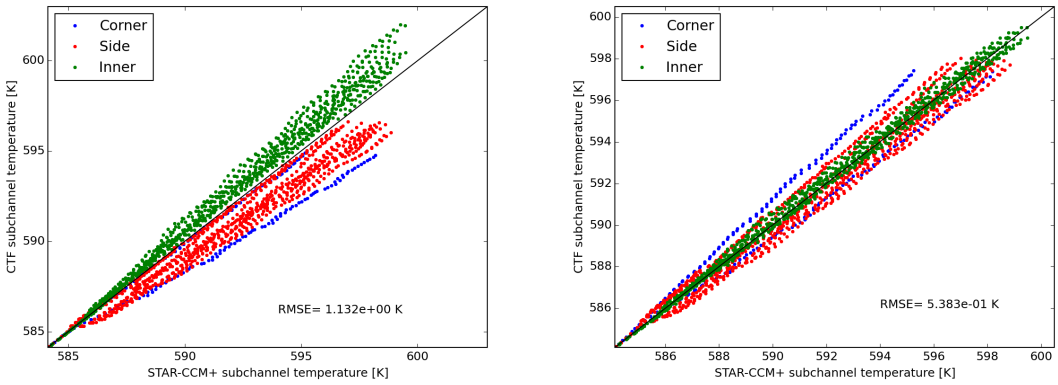

(a) β=0.005.

(b) β = 0.037.

Fig. 4. Comparison of STAR-CCM+ and CTF subchannel temperature distribution prediction.

refinement), 2×2, 4×4, 8×8, and 16×16. CTF will perform a numerical integration of the supplied CFD data onto the coupling mesh faces. The following comparison is made for the center rod in the 5×5 facility.

The supplied ROTHCON map has 16 data points per CTF rod sector and over 50 data points per CTF axial rod level. The comparison is done by remapping the coupling mesh multipliers calculated by CTF onto the supplied map mesh using a direct, nearest neighbor interpolation. The root-mean-square error (RMSE) of the difference between all data points is then taken, as shown in Equation 3, where N is the total number of data points in the supplied map (and remapped CTF coupling mesh map), and M is the multiplier. The results of the coupling mesh refinement are shown in Figure 5.

$$\text{RMSE} = \sqrt{\Sigma_{n=1}^{N}(M_{\text{CTF}} - M_{\text{supplied}})^2/N} \tag{3}$$

The rate of improvement slows when moving to the 16×16 refinement because the coupling mesh refinement is on the same order as the supplied mesh. The improvement in the coupling mesh resolution of the supplied multiplier map can also be seen in Figure 6.

The multiplier map refinement comparison helps to verify that the mesh remapping is working correctly in CTF. An additional refinement study was performed in which the predicted CTF temperatures on the coupling mesh using the ROTHCON reconstruction were compared to the original STAR-CCM+ data that were used to generate the HTC multiplier map. The same refinement levels that were used for the multiplier map study were used for the temperature reconstruction study. Figure 7 shows the results. The results seem to asymptotically approach an error of 0.4–0.6 K. As shown in Figure 4, the RMSE of

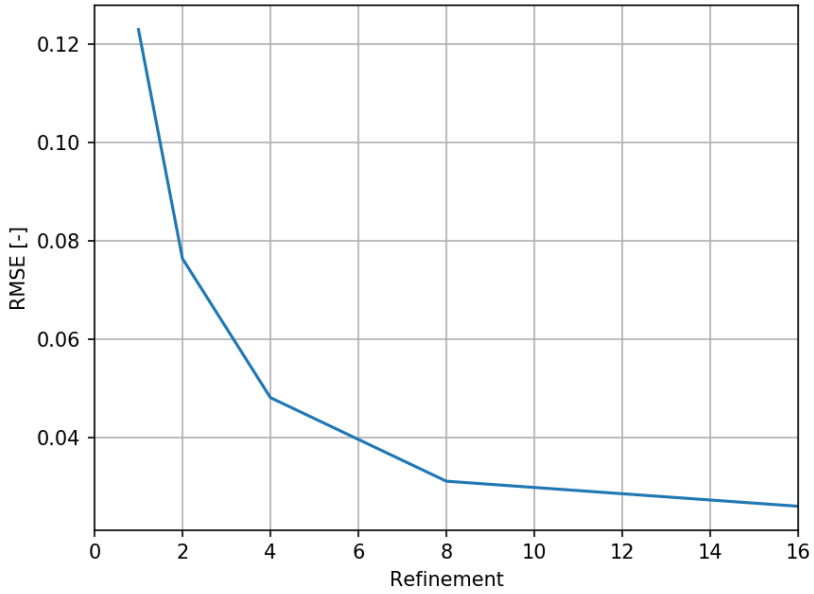

Fig. 5. RMSE of the differences between the coupling mesh multiplier map and the multiplier map supplied to CTF. The results show that the error between the two maps continues to reduce as the coupling mesh is refined.

the difference between CTF and STAR-CCM+ channel fluid temperature predictions is about 0.5 K. The fluid temperature will have a direct impact on predicted rod surface temperature, so this error will limit the degree to which the rod surface temperature predictions may be improved.

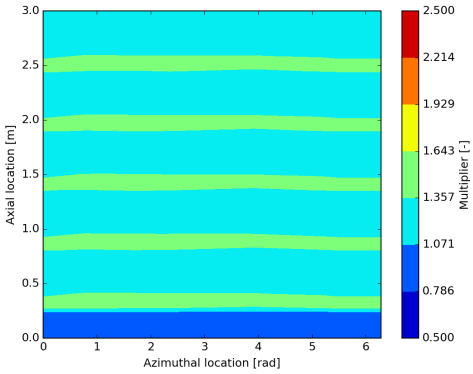

(a) Coupling mesh multiplier map using 1×1 refinement

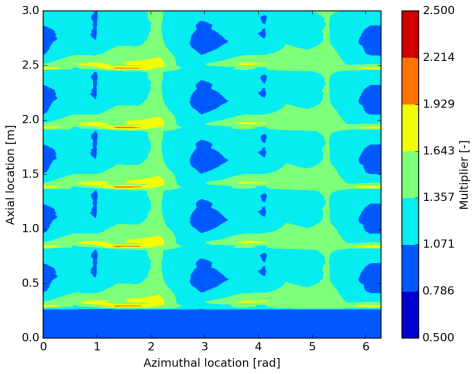

(b) Coupling mesh multiplier map using 4×4 refinement

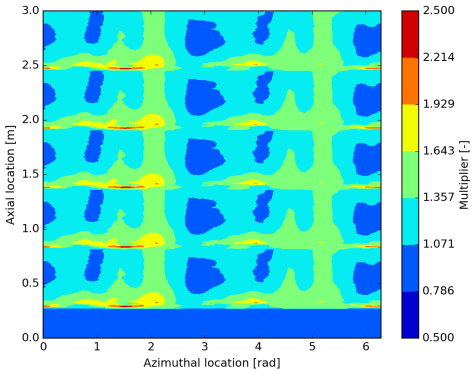

(c) Coupling mesh multiplier map using 16×16 refinement

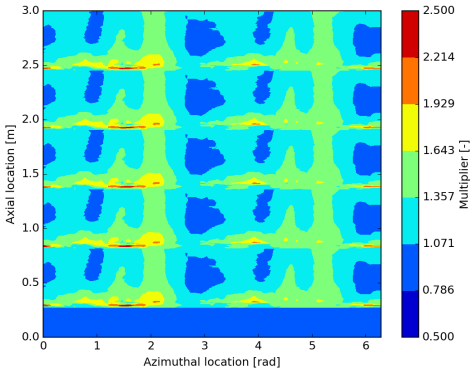

(d) Supplied multiplier map

Fig. 6. Comparison of supplied map and coupling mesh map for HTC multiplier

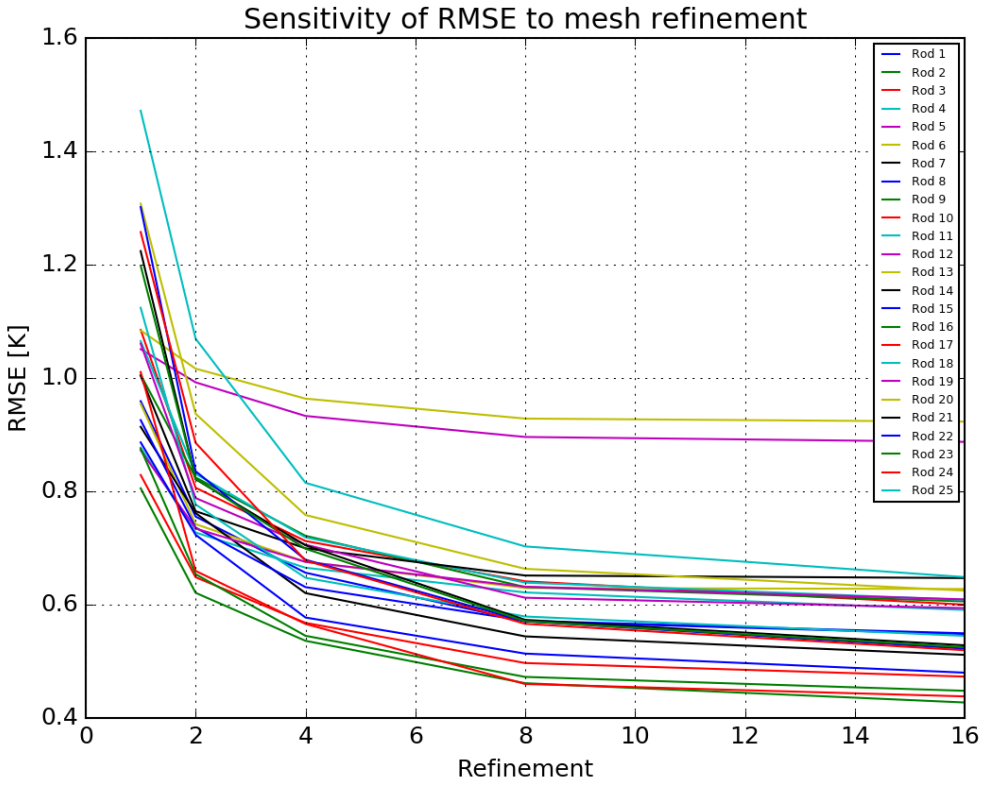

Fig. 7. RMSE of the difference between STAR-CCM+ rod surface temperature predictions and CTF rod surface temperature predictions using the ROTHCON process. A single RMSE is calculated for each rod at each level of coupling mesh refinement. Adjacent subchannel temperatures of corner rods 5 and 13 compare less favorably with STAR-CCM+, leading to less of an improvement for those rods. The RMSE of the difference between CTF and STAR-CCM+ channel temperature predictions is 0.5 K.

IV.B. Nominal case assessment

Figures 8(a) and 8(b) show STAR-CCM+- and CTF-predicted rod surface temperatures for Rods 1 and 25 of Case 0. Each point in the figure represents a unique cell that intersects with the rod's surface. The CTF results were obtained by averaging the four quadrants of the rod to a single value.

The CTF rod surface temperatures tend to over predict the STAR-CCM+ results because no grid heat transfer model was employed when generating these results. However, even if a traditional grid model were applied, then the fine azimuthal temperature distribution would not be captured. As the results indicate, this azimuthal variation can be as much as 5 K. These results also show that there is no boiling in this test case. This is desirable because it is preferable not to capture boiling heat transfer effects in the shape function. Boiling heat transfer is a function of local T/H conditions and must be calculated by CTF.

Figure 9 shows heat transfer coefficients for two arbitrary rods, Rods 5 and 12, in Case 0. As observed from the figures, the heat transfer behavior on different rod surfaces can be quite different. This makes it difficult to develop a more general purpose rod heat transfer model that applies to all rods. However, the figures also reveal that the heat transfer behavior in the axial direction is very consistent when the inlet spans—where flow is still developing—are neglected. Therefore, the approach taken was to select one span as a reference span. The second full grid span was selected because flow behavior was well established by this span. This was then used to model heat transfer behavior in all other spans in the CTF model. The heat transfer behavior of all rods is captured in the multiplier map for the given span. This has a drawback of requiring a STAR-CCM+ model to be run for the entire lateral domain of the assembly. However, the benefit is that only a single span, plus ample upstream length for flow development, must be modeled.

Three comparisons were made for Case 0 results: (1) CTF with no grid model, (2) CTF with the STAR-CCM+ produced model, and (3) CTF with the YHL model using a blockage ratio of 35 %. This blockage ratio was not calculated from the grid geometry, but it is a typical blockage ratio for a very dense grid. For all comparisons, the inlet region (region upstream of the first grid) is not included in the comparison. Rod 25 (the center rod) is selected to show the effect of the HTC map. These results are shown in Figure 10.

As the figures indicate, rod surface temperatures are substantially over predicted by CTF everywhere when a grid heat transfer model is not applied. The YHL model improves predictions by decreasing the RMSE, particularly in the regions just downstream from the grid. However, the YHL model under predicts

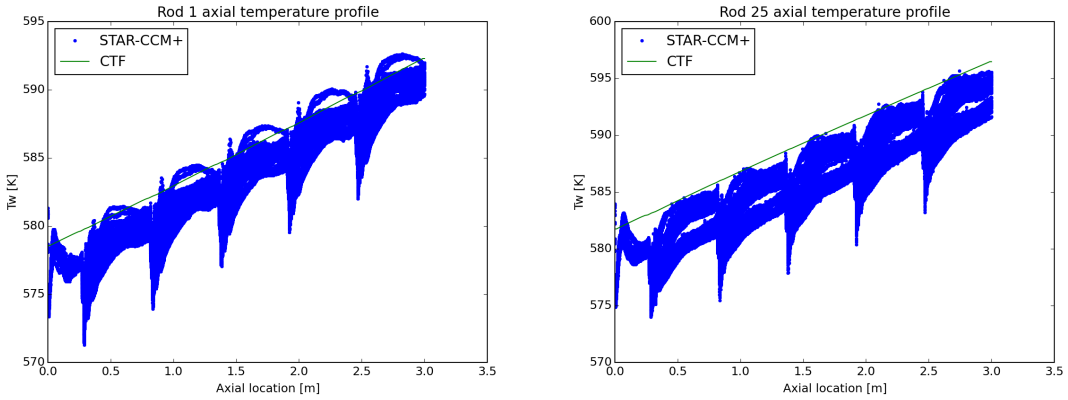

(a) Rod 1. (b) Rod 25.

Fig. 8. Comparison of STAR-CCM+ and CTF rod surface temperature distributions for Case 0.

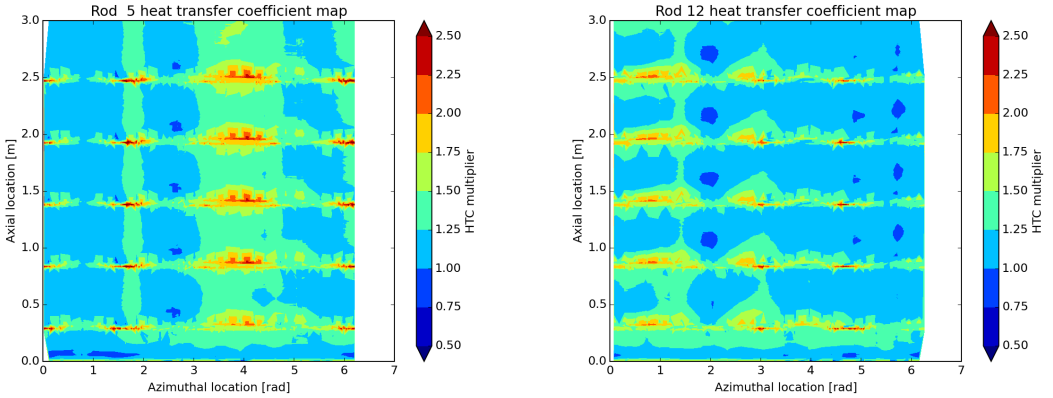

(a) Rod 5. (b) Rod 12.

Fig. 9. STAR-CCM+-calculated HTC multiplier maps for two rods in the 5×5 geometry.

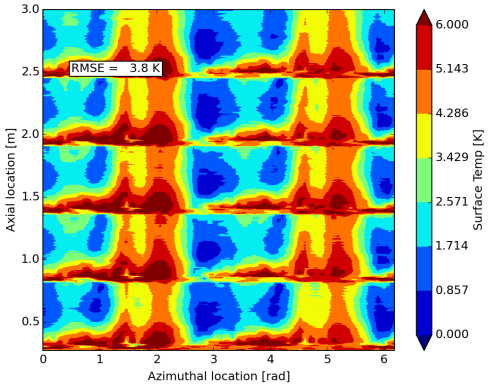

(a) No model.

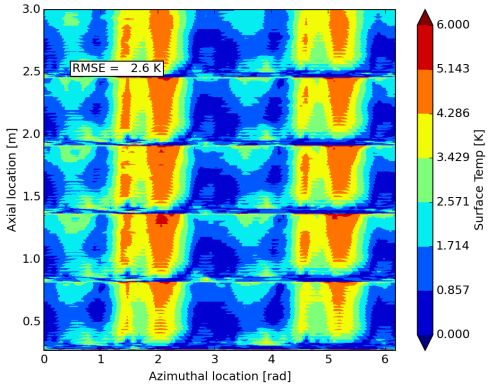

(b) YHL model.

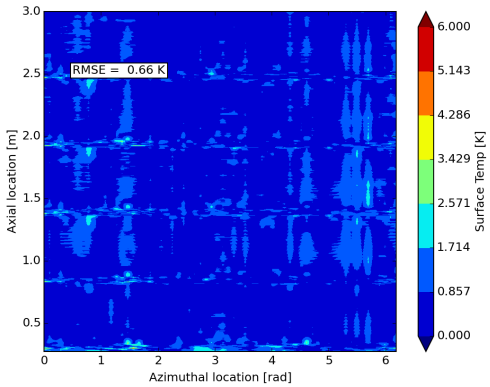

(c) STAR-CCM+ model.

Fig. 10. Absolute difference between STAR-CCM+ temperature distribution and CTF temperature distribution for Rod 25 (Case 0).

the true heat transfer enhancement behavior of the grid, particularly in the regions far downstream from the grid. Additionally, the YHL model cannot capture azimuthal heat transfer effects, which can vary significantly because of mixing vane effects. Applying the HTC multiplier maps that were generated from the STAR-CCM+ results improved agreement with STAR-CCM+.

IV.C. Boundary Condition Assessment

For ROTHCON to be useful, it must successfully reconstruct rod surface T/H data for flow, temperature, and power conditions other than the ones used to create the multiplier map. The multiplier map that was developed for Span 2 of Case 0 was used to reconstruct rod surface temperature for the other cases in Table I. Statistics were generated in the same way as was done in Section IV.A. Figure 11 provides a summary of the improvement in rod surface temperature predictions for all rods in the assembly. The RMSE is used to summarize the discrepancy with STAR-CCM+ results. The results indicate a substantial improvement in agreement between CTF and STAR-CCM+ for the rod surface temperature for all cases. The results also indicate that the multiplier map is fairly independent of inlet temperature and flow. There does seem to be a slightly larger effect of power shape, and especially a presence of subcooled boiling, on level of improvement, as Case 4 and 5 RMSE are generally slightly larger than RMSE for all other cases. Regardless of this, discrepancy between CTF and STAR-CCM+ temperature predictions is substantially reduced for all cases tested.

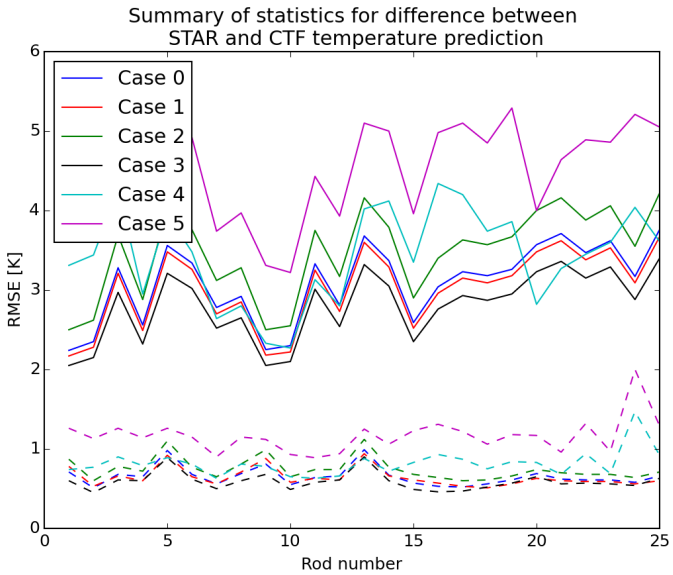

Fig. 11. RMSE of the absolute difference between CTF and STAR-CCM+ rod surface temperature predictions for all rods in all cases. Solid lines represent cases with no grid heat transfer model, and dashed lines represent cases with the STAR-CCM+ grid heat transfer model generated from Case 0 applied.

V. CONCLUSION

An approach called ROTHCON was developed and demonstrated for mapping grid-induced heat transfer behavior from high-fidelity CFD results to lower fidelity subchannel simulations as a shape function. It was found that grid heat transfer effects are generally very repeatable in the axial direction, but they vary considerably from rod to rod. Therefore, an approach was taken in which a single span was used to define an HTC multiplier map that applies to all rods in the bundle in that span. This reference span is then applied for each span in the subchannel model where that grid design is encountered.

Before generating and implementing the HTC maps, the CTF solution was compared to subchannel-averaged STAR-CCM+ results, and CTF models were calibrated to better match the STAR-CCM+ subchannel-averaged results. A STAR-CCM+ rod bundle simulation was then used to generate a grid HTC multiplier map. CTF was modified to be able to read this map and to use it to calculate the rod temperature distribution on a refined rod mesh that is used for coupling to MAMBA. This reconstructed temperature distribution was compared to CTF-predicted temperatures using the traditional YHL grid heat transfer model and no heat transfer model. It was found that the STAR-CCM+–generated maps led to considerable improvement in prediction of rod surface temperature distribution by CTF when compared to CFD, having RMSEs that are

often 3–5 times lower than using no model or YHL. As results have shown, the grid effect on heat transfer can often be seen throughout the entire span, which is not as well captured by the YHL model. This can lead to over prediction of crud thickness in regions that typically have high CIPS risk. No comparison was made against experimental data during this study as the emphasis was only on demonstrating the validity of the approach to reconstruct CFD data in a subchannel code. Work is ongoing to improve the usability of this feature and to assess it for larger scale assemblies using commercial spacer grid designs. Future work is also planned to quantify the STAR-CCM+ uncertainty and improve on the present process so that the uncertainty may be propagated through to the rod quantity surface calculations.

ACKNOWLEDGMENTS

This research was supported by the Consortium for Advanced Simulation of Light Water Reactors (www.casl.gov), an Energy Innovation Hub (http://www.energy.gov/hubs) for modeling and simulation of nuclear reactors under U.S. Department of Energy Contract No. DE-AC05-00OR22725.

This research used resources of the Oak Ridge Leadership Computing Facility at the Oak Ridge National Laboratory, which is supported by the Office of Science of the U.S. Department of Energy under Contract No. DE-AC05-00OR22725.

ACRONYMS

BWR boiling water reactor

CAD computer-aided drafting

CASL Consortium for Advanced Simulation of Light Water Reactors

CILC crud-induced localized corrosion

CFD computational fluid dynamics

CIPS crud-induced power shift

DNB departure from nucleate boiling

HTC heat transfer coefficient

LWR light water reactor

PWR pressurized water reactor

RIA reactivity insertion accident

RMSE root-mean-square error

ROTHCON rod thermal-hydraulic reconstruction

T/H thermal-hydraulics

YHL Yao-Hochreiter-Leech

REFERENCES

[1] R. SALKO, A. WYSOCKI, M. AVRAMOVA, A. TOPTAN, N. PORTER, T. BLYTH, C. DANCES, A. GOMEZ, C. JERNIGAN, and J. KELLY, *CTF Theory Manual*, The North Carolina State University (2017).

[2] M. THURGOOD, J. KELLY, T. GUIDOTTI, R. KOHRT, and K. CROWELL, "COBRA/TRAC - A Thermal-Hydraulics Code for Transient Analysis of Nuclear Reactor Vessels and Primary Coolant Systems Equations and Constitutive Models," NUREG/CR-3046, PNL-4385, Pacific Northwest National Laboratory (1983).

[3] B. KOCHUNAS, B. COLLINS, S. STIMPSON, R. SALKO, D. JABAAY, A. GRAHAM, Y. LIU, K. S. KIM, W. WIESELQUIST, A. GODFREY, K. CLARNO, S. PALMTAG, T. DOWNAR, and J. GEHIN, "VERA Core Simulator Methodology for Pressurized Water Reactor Cycle Depletion," *Nuclear Science and Engineering*, **185**, *1*, 217 (2017); 10.13182/NSE16-39., URL https://doi.org/10.13182/NSE16-39.

[4] B. COLLINS, J. GALLOWAY, R. SALKO, A. WYSOCKI, K. CLARNO, B. OKHUYSEN, S. SLATTERY, N. ADAMOWICZ, D. ANDERSEN, D. POINTER, A. MANERA, B. KENDRICK, W. GURECKY, V. PETROV, B. WIRTH, and J. RIZK, "Development of a Comprehensive CRUD-Induced Power Shift (CIPS) Capability within VERA," CASL-X-2017-1406-000, Consortium for Advanced Simulation of Light Water Reactors (2017).

[5] S. SLATTERY, R. SALKO, and K. CLARNO, "The Effect of Subchannel vs. CFD Discretizations on CRUD Growth using MAMBA1D," , Consortium for Advanced Simulation of Light Water Reactors (2015).

[6] D. WALTER, V. PETROV, A. MANERA, B. KENDRICK, and R. SALKO, "Two-Phase CFD/Subchannel Comparison and Assessment of the MAMBA CRUD Deposition Models L2.THM.P13.01," CASL-U-2016-1242-000, Consortium for Advanced Simulation of Light Water Reactors (2016).

[7] S. YAO, L. HOCHREITER, and W. LEECH, "Heat-Transfer Augmentation in Rod Bundles Near Grid Spacers," *Journal of Heat Transfer*, **104**, 76 (1982).

[8] T. BLYTH and M. AVRAMOVA, "Development and Implementation of CFD-Informed Models for the Advanced Subchannel Code CTF," CASL-U-2017-1308-000, Consortium for Advanced Simulation of Light Water Reactors (2017).

[9] R. SALKO, W. GURECKY, S. SLATTERY, K. CLARNO, D. POINTER, D. WALTER, V. PETROV, and A. MANERA, "Implementation of a Grid Heat Transfer and Turbulent Kinetic Energy Hi2Lo Remapping Capability into CTF in Support of the CIPS Challenge Problem," CASL-U-2017-1322-000, Consortium for Advanced Simulation of Light Water Reactors (2017).

[10] D. POINTER, "Reference Computational Meshing Strategy for Computational Fluid Dynamics Simulation of Departure from Nucleate Boiling," CASL-U-2017-1390-000, Consortium for Advanced Simulation of Light Water Reactors (2017).

[11] "Description of Mixing Vane Grid CHF test for CASL DNB Challenge Problem," PFT-16-3, Rev.1 (Westinghouse Proprietary) (2016).

[12] R. SALKO, M. DELCHINI, X. ZHAO, D. POINTER, and W. GURECKY, "Summary of CTF Accuracy and Fidelity Improvements in FY17," CASL-U-2017-1428-000, Consortium for Advanced Simulation of Light Water Reactors (2017).

[13] N. GORDON, L. GILKEY, T. BLYTH, R. SMITH, E. TATLI, and Y. SUNG, "Initial Application of Hi2Lo Approach to Turbulent Mixing Model Improvement L3:AMA.CP.P14.04," CASL-X-2017-1292-000, Consortium for Advanced Simulation of Light Water Reactors (2017).

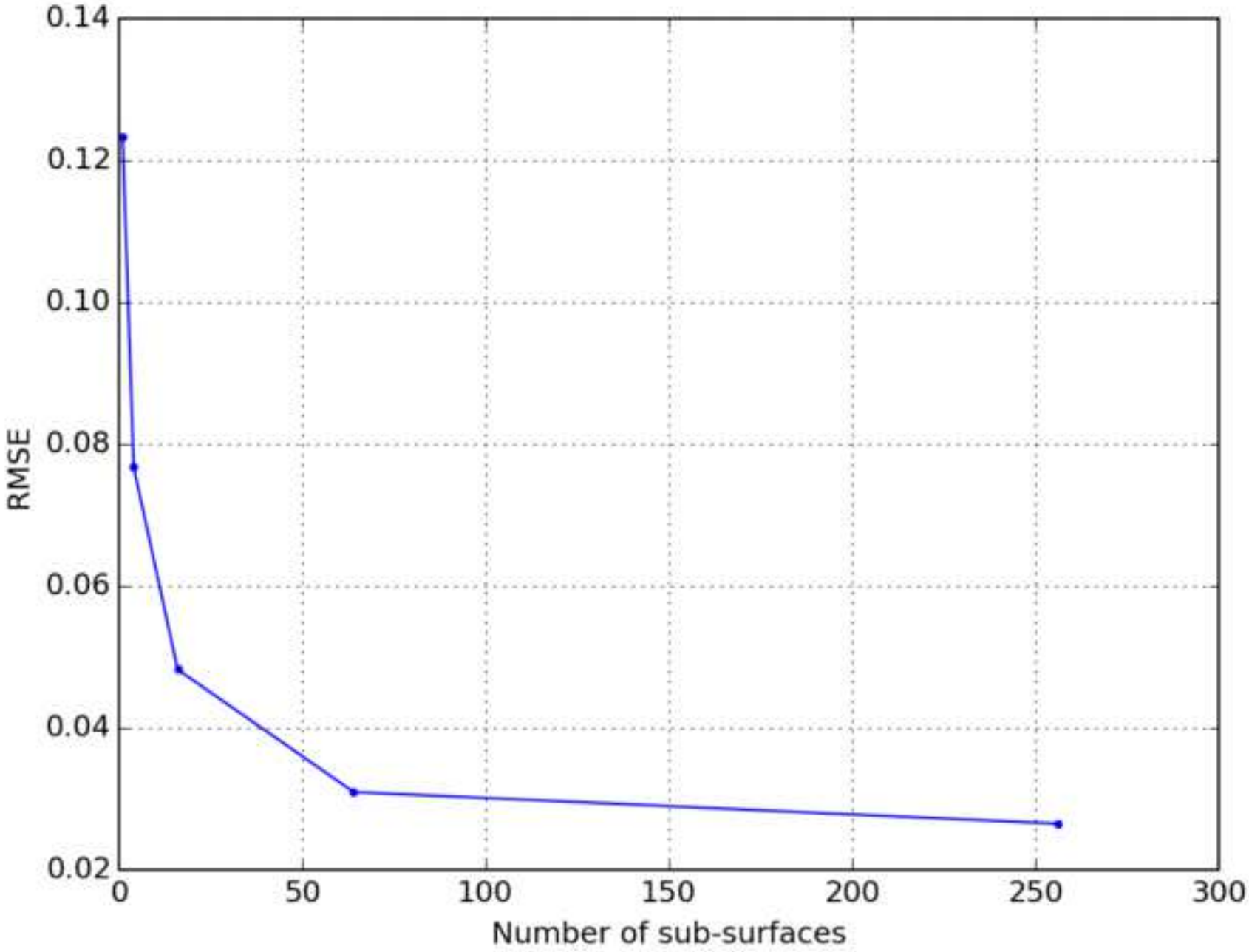
0.14
0.12
0.10
0.08
0.06
0.04
0.02
RMSE
0
50
100
150
200
250
300
Number of sub-surfaces